Problem-matched basis functions for microstrip coupled slot antennas based on Transmission Line Green's Functions (TLGF)

Problem-Matched Basis Functions for Microstrip Coupled Slot Arrays Based on Transmission Line Green's Functions (TLGF)

Simona Bruni, Nuria Llombart, Andrea Neto, *Member, IEEE*, Giampiero Gerini, *Member, IEEE*, and Stefano Maci, *Fellow, IEEE*

***Abstract*—Problem matched basis functions are proposed for the method of moments analysis of printed slot coupled microstrips. The appropriate equivalent currents of the integral equation kernel are represented in terms of two sets of entire domain basis functions. These functions synthesize on one hand the resonant behavior of slots, microstrips or dipoles and on the other hand the field in proximity of the feeding source and of the discontinuities. In order to define these basis functions, canonical geometries are identified, whose Green's functions have been found in semi-analytical form. The accuracy and the effectiveness of the method in terms of convergence rate and number of unknowns is demonstrated by comparison with a standard fine meshing full-wave analysis. The method is extremely convenient for large arrays, where the subwavelength details should be treated together with large global dimensions. Since the proposed solution is independent of the dimensions of these details, it provides dramatic reduction of the number of unknowns and improvement of condition number.**

***Index Terms*—Entire domain basis functions, Green's functions, method of moments (MoM).**

I. Introduction

ARRAY antenna modeling is a challenging issue, since it involves large structures (in terms of the wavelength), as well as fine details that require discretizations much-smaller than wavelength, and that dominate the frequency response of input parameters. The integral equation (IE) approach is largely used to analyze these problems, through the method of moments (MoM) discretization scheme. It is well-known, however, that standard techniques are severely limited by the matrix size and condition number involved in the problems of interest. In these problems, the structure of the solution exhibits very different scales of variation; for examples, local interactions in a geometry, subwavelength details, edges and discontinuities, generate small-scale details of high spatial frequency, while distant interactions as well as resonant lengths are responsible for the low-frequency, slow spatial variations. One is typically forced to choose mesh cells of size comparable to the smallest foreseen scale of the solution, i.e., with the highest possible spatial resolution. Unfortunately, this leads to a large number of unknowns, densely populated MoM matrices with a poor condition number, and renders the direct approach of large problems numerically intractable.

A number of techniques have been presented in the past years to overcome the difficulties mentioned above, whose review is outside the scopes of this work. Let us just mention some of the methods which lead to a compression of the MoM size based on either physical or numerical schemes. Among the numerically based methods, we point out the fast multiple method [1], the multilevel matrix decomposition algorithm [2] and the multi resolution method [3]. Physical based approaches which exhibit some common features are the truncated Floquet wave (TFW) method [4]–[7], the synthetic basis function expansion (SFX) method [8]–[11] and the characteristic basis functions (CBF) method [12], [13]. These methods attempt to keep explicit information about the multiscale nature of the solution directly into the representation of the unknown currents. These approaches can be applicable to quite general array geometries, with (possibly) different radiators. In any case, even if with different approaches, the complexity is reduced by compressing a (large) matrix. Despite the fact that these have been shown to be very successful they may possess a margin of improvement for certain typology of array problems.

In this paper we present a method framed in the same philosophy but based on the quasianalytical form of transmission line Green's function (TLGF). Even if limited to array elements constituted by pieces of slot-line, microstrip-line, dipoles and their relevant coupling, the present method allows the analytical derivation of the basis functions, thus simplifying the preprocessing phase and gaining physical insight. It is the extension and the systematization to multilayered arrays and relevant microstrip, or slotted, beam forming networks (BFN) of the pioneering technique presented in [14]. The applicability of this latter was limited to the case in which slots or coplanar wave-guides were printed between two homogeneous infinite dielectrics because in that specific case the GF was found analytically [15]. Such limitation is removed in this paper, by using an efficient precalculation of the structural GF for the relevant transmission line.

Manuscript received May 6, 2004; revised May 9, 2005.

S. Bruni is with TNO Defence, Safety and Security, Den Haag 2597 AK, The Netherlands, and also with the Department of Information Engineering, University of Siena, 53100 Siena, Italy (e-mail: simona.bruni@tno.nll; bruni@dii.unisi.it).

A. Neto and G. Gerini are with TNO Defence, Safety and Security, Den Haag 2597 AK, The Netherlands (e-mail: andrea.neto@tno.nl; giampiero.gerini@tno.nl).

N. Llombart is with TNO Defence, Safety and Security, Den Haag 2597 AK, The Netherlands, and also with the Departamento de Comunicaciones, Universidad Politécnica de Valencia, E-46022 Valencia, Spain (e-mail: nuria.llombartjuan@tno.nl).

S. Maci is with the Department of Information Engineering, University of Siena, 53100 Siena, Italy (e-mail: macis@ing.unisi.it).

Digital Object Identifier 10.1109/TAP.2005.858581

The entire domain basis functions are generated by solving in quasianalytical form some specific TLGF problems with an appropriate chosen excitation. Each basis function is thus solution of an integral equation which represents the boundary condition of a physical problem; consequently, they have the adequate content of local reactive energy, and include a good approximation of the right transverse edge behavior. Indeed, as demonstrated here, the present method allows the reduction of the number of unknowns while preserving accuracy. Moreover, it implies a substantial improvement of the condition number, due to the small MoM matrix size and to the fact that strong variations of the field are intrinsically described without the need of many small subdomain basis functions. Physical insight is also gained, since each one of the basis function can be associated with a specific electromagnetic GF-problem which is essentially regulated by well distinct wave contributions. These contributions are of travelling wave type and fringe type; the latter are associated to reactive energy stored close the feed-point and, due to their large spectral contents, dominate the short range coupling. The travelling wave basis functions dominate the large distance coupling; this allows to establish a robust criterion to select the essential large distance contributions of the MoM matrix, thus drastically improving the filling time especially for medium to large arrays. The advantages are particularly impressive for cases in which the specific shape of the feed details are small in terms of a wavelength and would tend to render cumbersome a sufficiently fine meshing. One of such examples is shown among the results. The procedure proposed in this paper can also be used as a matrix-compression technique when the basis function are viewed as ruling the grouping of the subdomain unknowns; this leads to the possibility to apply the present method in the framework of a conventional subdomain algorithm by reusing already available codes. This aspect of this approach is in common with the TFW method or the SFX method. It is finally worth mentioning that, despite the limitation to arrays built from combinations of pieces transmission lines that are thin in terms of wavelength, a large variety of practical problem requires printed dipoles and slots which are fed by BFN composed by microstrip, CPW, slot lines.

The presentation of this paper is structured as follows. Section II summarized a general methodology to derive the equivalent currents associated to the TLGF. The general solution is then particularized to the cases of microstrips (excited by δ-gap or by a magnetic current source) and slots (excited by an electric current source). In Section III the TLGF is first represented in terms of a residue of a spectral pole and a "fringe" contribution. Then, the entire domain basis functions associated to these two contributions are introduced. In Section IV the application to resonant and nonresonant arrays is shown. Conclusions are drawn in Section V.

II. Printed TLGF

This section describes the TLGF relevant to a source in the presence of an infinite guiding structure printed on a general multilayered dielectric media. The formulation is substantially an extension of that employed in [15] which is based on the method proposed in [17], and their cited references. The examined structures are:

- slots etched on an infinite ground plane; in this case the unknown currents are of magnetic type and will be denoted by m;
- strips printed at the interface between dielectric slabs (dipoles, microstrips, etc.); in this case the unknown currents are of electric type and will be denoted by j.

For the sake of generality in this section the unknown equivalent current will be indicated as c. The result will be specified for $c = j$ and $c = m$ in the subsequent sections. The unknown current is assumed as oriented along the longitudinal direction l; the transverse direction is indicated by the variable t. In Section II-B, we will specifically refer to $(l, t) = (x, y)$ or $(l, t) = (y, x)$ for slot or microstrip, respectively. The width w_t of the guiding structure is assumed to be small in terms of the wavelength, so that the separation of the variables l and t can be invoked for the space dependence of the current

$$c(l,t) = \epsilon c_l(l) p_t(t) \hat{l}. \tag{1}$$

In (1), $\hat{l}$ is the unit vector along the longitudinal variable l and ϵ is equal to 1 in the slot cases and -1 in the microstrip cases.

The transverse function $p_t(t)$ is assumed known *a priori*, such as to verify the edge singularity condition

$$p_t(t, w_t) = \frac{2}{w_t \pi} \frac{1}{\sqrt{1 - \left(\frac{2t}{w_t}\right)^2}}. \tag{2}$$

In (2) $t = 0$ is assumed to be in the center of the microstrip or of the slot depending on the problem one is considering and the corresponding local reference system. The normalization constant $(2/(w_t\pi))$ has been chosen in such a way that $c_l(l)$ in (1) represents voltage or current for slot or microstrip. The function $p_t(t, w_t)$ possesses a closed-form Fourier transform

$$P_t(k_t, w_t) = \mathrm{FT}\left\{p_t(t, w_t)\right\} = J_0\left(\frac{1}{2} w_t k_t\right). \tag{3}$$

where J_0 is the Bessel function of zero order. It is worth noting that if the transverse distribution was assumed to be constant, rather than edge singular the GF derivation would not have varied significantly and only a small differences in the actual propagation constants values would have been found. In general (2) can be used safely as long as the cross section is smaller then a tenth of the wavelength in the denser dielectric. The expression represents the first order approximation of the exact solution for the electric field in a narrow slot excited by a plane wave incidence, [18].

The pertinent integral equation is now set up. For both types of structure either the continuity of magnetic field integral equation (CMFIE) or the electric field integral equation (EFIE) can be placed in the following form:

$$f^s(l,t) = -f^i(l,t) \tag{4}$$

where the field f can be either the electric or the magnetic field component (for microstrip or slot problems, respectively) along the longitudinal direction. The superscripts i and s indicates the

incident and scattered field, respectively. The scattered field is conveniently expressed in a spatial convolution form as

$$f^s(l,t)=\int_{-\infty}^{+\infty}\int_{-w_t/2}^{w_t/2} g_{ll}(l,l',t,t',z_0)c_l(l')p_t(t',w_t)dt'dl'. \tag{5}$$

Where g_{ll} is the pertinent GF of the environment. This GF is associated to magnetic field and magnetic dipole or to electric field and electric dipole in absence of the guiding structure and in presence of the dielectric stratification. The first step of the solution procedure is the Galerkin projection of (4) onto a transverse test function $p_t(t)$. This leads to an equation where the unknown depends on the longitudinal dimension only. By transforming then both the left-hand side (LHS) and the right-hand side (RHS) in the Fourier (k_l,k_t) domain, we obtain

$$\begin{aligned}&\int_{-\infty}^{+\infty}\int_{-\infty}^{+\infty} G_{ll}(k_l,k_t)C_l(k_l)P_t(k_t,w_t)P_t(-k_t,w_t)\\&\quad\times e^{-jk_ll}dk_ldk_t\\&\qquad=-\int_{-\infty}^{+\infty}\int_{-\infty}^{+\infty} P_t(-k_t,w_t)F^i(k_l,k_t)e^{-jk_ll}dk_ldk_t.\end{aligned} \tag{6}$$

Where G_{ll}, F^i, and C_l are the Fourier transforms of g_{ll}, f^i and c_l, respectively. Since (6) is valid for all values of l, we may impose the equality of the k_l spectra. By defining

$$N(k_l)=-\int_{-\infty}^{+\infty} P_t(-k_t,w_t)F^i(k_l,k_t)dk_t \tag{7}$$

and

$$D(k_l)=\int_{-\infty}^{+\infty} G_{ll}(k_l,k_t)P_t(k_t,w_t)P_t(-k_t,w_t)dk_t \tag{8}$$

the longitudinal variation of the current can be compactly expressed as

$$c_l(l)=\frac{1}{2\pi}\int_{-\infty}^{+\infty}\frac{N(k_l)}{D(k_l)}e^{-jk_ll}dk_l. \tag{9}$$

In few cases (e.g., slot printed on a ground plane which separate two semi-infinite media), the current spectra may be evaluated in analytical form [15], [16]. In the general case this is not possible; however, the spectrum in (9) possesses some analytical properties which are very useful to improve the efficiency by physical association of the analytical contributions.

A. Travelling and Fringe Contributions to the GF

It is significant to separate large k_l and small k_l spectral contributions as associated to different physical contents in the space domain. The asymptotic (large k_l) parts of the spectra are typically associated to reactive energy stored in the surrounding of the source. The small k_l spectral contributions are instead associated to propagation and radiation phenomena. As such, they are responsible for mutual coupling between different part of the actual possibly nonrectilinear structure. In particular the lower portion of the k_l spectra is dominated by spectral poles arising from the zero of $D(k_l)$ in (8). These poles represent bound modes or leaky waves modes when properly extracted as residues. For general configurations the number of poles is not limited. As the frequency becomes higher there will be more modes excited. However, in the practical case of a microstrip with small width and thin dielectric slabs only one couple of significant poles located in $\pm k_{lp}$ occur. The same happens with small slots printed on thin dielectric slabs or on infinite dielectric substrates. The localization of these poles as a function of the parameters of the structure, can be performed numerically once a good initial guess (β_l) is assumed. The initial guess can be given by any of the quasistatic approximations found in handbooks, like those simply derived by the geometrical average of the electric permittivities. However as outlined in [15], the approximation based on a one step iteration of the Newton method

$$k_{lp}\simeq\beta_l-\frac{D(\beta_l)}{D'(\beta_l)} \tag{10}$$

is accurate enough to approximate the spectral pole for small TL width and, in any case, constitutes an excellent initial guess, also for complex values of k_{lp}. Once one has found k_{lp}, it is convenient to regularize the spectrum by extracting the function

$$C_{tw}(k_l)=\frac{2k_{lp}N(k_{lp})}{D'(k_{lp})\left(k_l^2-k_{lp}^2\right)} \tag{11}$$

whose inverse transform leads to the space domain dynamic contribution $c_{tw}(l)$. Accordingly, the overall unknown currents can be systematically expressed as a summation of two contributions:

$$c_l(l)=c_{fr}(l)+c_{tw}(l) \tag{12}$$

where

$$c_{fr}(l)=\frac{1}{2\pi}\int_{-\infty}^{+\infty}\left(\frac{N(k_l)}{D(k_l)}-C_{tw}(k_l)\right)e^{-jk_ll}dk_l \tag{13}$$

and

$$c_{tw}(l)=\frac{1}{2\pi}\int_{-\infty}^{+\infty}C_{tw}(kl)e^{-jk_ll}dk_l. \tag{14}$$

We will refer to the term $c_{fr}(l)$ as "fringe" current contribution as it is the remainder current once the dynamic (travelling) contribution $c_{tw}(l)$ has been extracted. The fringe current contribution can only be evaluated numerically except for few cases in which analytic expressions are available [15]. The dynamic contribution, instead, can always be evaluated analytically, by using the Jordan Lemma (note that the use of this lemma is legitimated by the regularity of the spectrum at infinity, which is a direct consequence of the radiation conditions). This leads to

$$c_{tw}(l)=\frac{-jN(k_{lp})}{D'(k_{lp})}e^{-jk_{lp}|l|} \tag{15}$$

which constitutes the leading asymptotic term of the current for l large and provides a good approximation for the total current at large distance from the source if losses in the structure are negligible. Otherwise, the bound-mode currents will decay exponentially, and it will be the continuous-spectrum current that is dominant at large distance from the source. In (15)

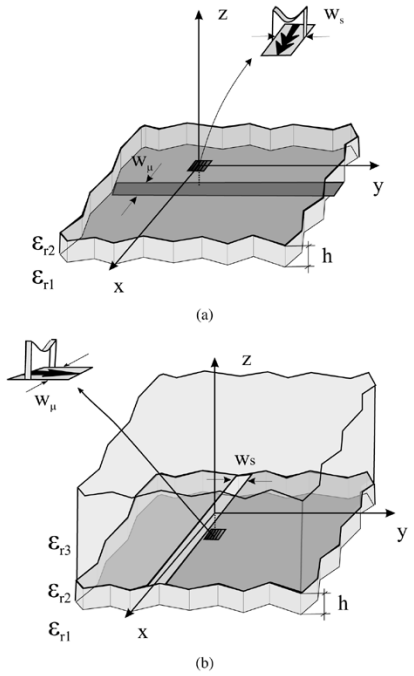

Fig. 1. Two canonical transmission line problems. (a) Infinite microstrip line excited by a magnetic dipole. (b) Infinite slot line excited by an electric dipole. In the inset dipole sources of width w_s and w_μ, used for deriving the basis functions.

$((-jN(k_{lp}))/(D'(k_{lp})))$ is the amplitude of the modal current of the wave launched in the structure. Depending on the real or complex nature of the pole, (15) represents a bound mode or a leaky wave mode. The leaky-wave poles to be extracted and used as basis functions are only those with small imaginary part, since the effects other ones is incorporated in the fringe effect.

B. Particular Cases: The Slot-Line and the Microstrip-Line

The treatment so far applies to all printed TLG characterized by a small transverse width; now we specialize the analysis to the two specific cases associated with the numerical examples presented in Sections III and IV.

Let us consider the two canonical structures shown in Fig. 1: (a) microstrip-line and (b) slot-line. The appropriate composition of the relevant solutions will allow the analysis of the mutual coupling of the cross over between slot and microstrip lines.

The y-oriented microstrip line is printed on a dielectric grounded slab (ϵ_{r2}, h) above a homogeneous dielectric (ϵ_{r1}) typically free-space [Fig. 1(a)]. The x-oriented slot is printed on an infinite ground plane which separates a homogeneous dielectric half-space of permittivity ϵ_{r3} $(z > 0)$ from an half space composed by a dielectric slab (ϵ_{r2}, h) followed by a semi-infinite uniform dielectric (ϵ_{r1}). The microstrip width (w_μ) and the slot width (w_s) are both small in terms of the wavelength. Without loss of generality we may assume $\epsilon_{r2} < \epsilon_{r3}$ and $\epsilon_{r1} = 1$. This is the common case for slot antennas, while for slot line the reverse case may be assumed without substantial difference. The slot is excited by a short electrical dipole while, the microstrip is excited by a short magnetic dipole, both arbitrary located at (x_0, y_0, z_0). Next, the

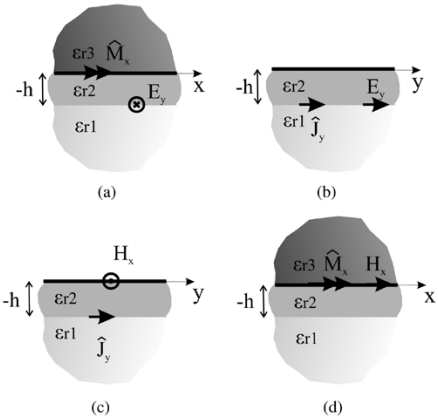

Fig. 2. Multilayer Green's functions for a magnetic and electric sources involved in (17)–(21). Arrow and double arrow represents electric and magnetic elementary dipoles, denoted by $\widehat{M}$ and $\widehat{J}$, respectively. (a) G_{yx}^{EM} in (17). (b) G_{yy}^{EJ} in (18). (c) G_{xy}^{HJ} in (20). (d) $G_{xx}^{HM\pm}$ in (21).

quantity defined in (7)–(9) are specified with reference to the two previous canonical problems.

1) Microstrip Transmission Line: Let us assume an excitation provided by a magnetic dipole source centered at (x_0, y_0, z_0). The electric current $j(y)$ is expressed by (9) as

$$j(y) = \frac{1}{2\pi}\int_{-\infty}^{+\infty} \frac{N_\mu(k_y)}{D_\mu(k_y)} e^{-jk_y(y-y_0)} dk_y \tag{16}$$

where $N_\mu(k_y)$ and $D_\mu(k_y)$ are given by

$$N_\mu(k_y) = \int_{-\infty}^{+\infty} P_t(-k_x, w_\mu) G_{yx}^{EM}(k_x, k_y, -h, z_0) e^{jk_x x_0} dk_x \tag{17}$$

and

$$D_\mu(k_y) = \int_{-\infty}^{+\infty} G_{yy}^{EJ}(k_x, k_y) P_t(k_x, w_\mu) P_t(-k_x, w_\mu) dk_x. \tag{18}$$

In (17) the GF G_{yx}^{EM} represents the spectral y component of the electric field at the interface radiated by an x-directed elementary magnetic dipole on the ground plane radiating in presence of an infinite grounded dielectric slab [Fig. 2(a)]. $G_{yy}^{EJ}(k_x, k_y)$ represents the spectral y-oriented electric field radiated by a y-oriented electric current when both source and observer are located at the dielectric air interface $z = -h$ [Fig. 2(b)]. When in place of an elementary dipole, we use a small distribution with width w_s [see inset of Fig. 1(a)] the current j are obtained by (16) with $N_\mu(k_y)$ multiplied by $P_t(k_y, w_s)$.

2) Slot Transmission Line: The longitudinal dependence of the magnetic current $m(x)$ are given by

$$m(x) = \frac{1}{2\pi}\int_{-\infty}^{+\infty} \frac{N_s(k_x)}{D_s(k_x)} e^{-jk_x(x-x_0)} dk_x \tag{19}$$

where $N(k_x)$ and $D(k_x)$ are

$$N_s(k_x) = \int_{-\infty}^{+\infty} P_t(-k_y, w_s) G_{xy}^{HJ}(k_x, k_y, 0, z_0) e^{jk_y y_0} dk_y \tag{20}$$

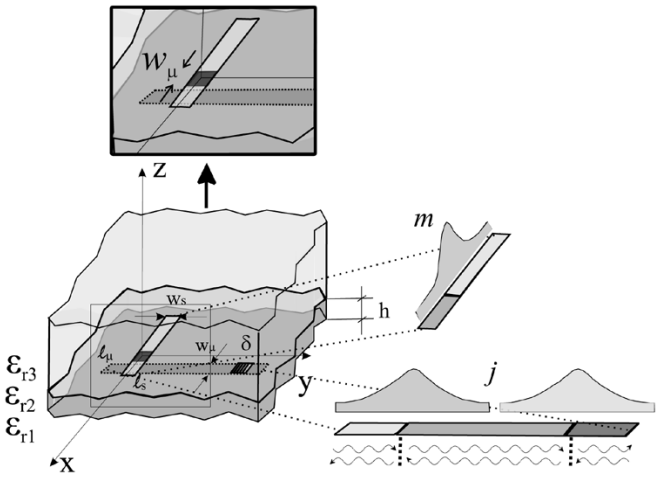

Fig. 3. Example of finite slot fed by a microstrip line. The discontinuity sections at the source and at the slot-microstrip crossing identify the boundary of the regions on which the unknown currents are described by travelling wave. Around the discontinuities additional fringe basis functions are defined, which incorporate the quasistatic field behavior. The dashed regions in the microstrip and in the slot identify the δ gap source and overlapping between the microstrip and the slot, respectively.

and

$$D_s(k_x) = \int_{-\infty}^{+\infty} \left(G_{xx}^{HM+}(k_x,k_y) + G_{xx}^{HM-}(k_x,k_y)\right) \times P_t(k_y,w_s)P_t(-k_y,w_s)dk_y \quad (21)$$

in (20) G_{xy}^{HJ} represents the spectral x component of the magnetic field radiated by an electric dipole in presence of an infinite dielectric slab of height h [Fig. 2(c)]. The Green's function for the slot case, contains two contributions; one $\left(G_{xx}^{HM+}\right)$ pertinent to upper $(z > 0)$ region and one $\left(G_{xx}^{HM-}\right)$ pertinent to the lower $(z < 0)$ region. Each one represents the x-oriented magnetic field radiated by an x-oriented magnetic current when both source and observer are located on the ground plane $z = 0$, Fig. 2(d).

III. Entire Domain GF-Based Basis Functions

The criteria and the operational procedure to derive the MoM basis functions are described with reference to a specific example of a single slot antenna fed by a microstrip; afterwards, the process can be generalized to more complex cases.

Consider the geometry in Fig. 3. The microstrip is excited via a δ-gap generator over a zone of length δ and width w_μ. The slot is electromagnetically coupled by the microstrip and a scattered current is induced on the microstrip by the slot. The first step is to divide the structure in portions free of discontinuities. With reference to Fig. 3, the microstrip can be divided in three regions by the two sections localized at the δ-gap generator and at the slot cross over. The slot can instead be divided in two regions by the cross-over with the microstrip. In each discontinuity-free region, the bulk of the unknown currents can be represented via travelling wave interference, while fringe functions are needed close to the section boundary between two regions. The explicit shape of these functions is given in the following. Before doing so we point out that it was found convenient to introduce a windowing $W(l)$ function that automatically tapers to zero the entire domain functions at the end of a transmission line domain. This provides the MoM procedure with a further degree of freedom associated to the fact that the entire domain basis functions intrinsically verify the null conditions when necessary.

A. Travelling Wave Basis Functions

The first type of basis functions we consider are the travelling waves. These functions may be parameterized by the propagation constant k_{lp} that coincides with the poles of the denominator in (18) and (21). Both a forward and a backward travelling waves are defined for each region. In the present test case the microstrip is divided in three regions while the slot is divided in two regions (Fig. 3). The actual expression of the forward and backward travelling waves in the ith region, centered in l_{ci} is given by

$$T_i^{\pm}(l,t) = e^{\mp jk_{lpi}(l-l_{ci})}p_t(t,w_t)W(l-l_{ci}) \quad (22)$$

where p_t is defined in (2), while the windowing function $W(l-l_{ci})$ imposes the appropriate null boundary conditions (NBC). Having defined the rectangular function as

$$\mathrm{rect}(l,l_i) = \begin{cases} 1, & \text{for } |l| < \frac{l_i}{2} \\ 0, & \text{for } |l| > \frac{l_i}{2} \end{cases} \quad (23)$$

the windowing function is written differently depending on if the NBC must be imposed on the left, on the right or it must not be imposed at all. In this latter case, for every block defining a domain, as

$$W(l-l_{ci},l_i) = \mathrm{rect}(l-l_{ci},l_i) \text{ for No NBC} \quad (24)$$

where l_i and l_{ci} are the length and the center of the ith block, respectively. In the case there is, for example, a right NBC condition the windowing function can be expressed as

$$W(l-l_{ci},l_i) = \mathrm{rect}\left[l - \left(l_{ex}^{+} - \Delta - \frac{l_i-\Delta}{2}\right), l_i - \Delta\right] + \mathrm{rect}\left[l - \left(l_{ex}^{+} - \frac{\Delta}{2}\right), \Delta\right]\sqrt{1 - \frac{l-(l_{ex}^{+}-\Delta)}{\Delta}} \quad (25)$$

where Δ is the space in which the basis function is forced to go to zero and l_{ex}^{+} is the right end coordinate of the ith block. Δ can assume two different values

$$\Delta = \frac{\lambda_{eq}}{4} \text{ if } l_i > \frac{\lambda_{eq}}{2}$$
$$\Delta = \frac{l_i}{2} \text{ if } l_i \le \frac{\lambda_{eq}}{2}. \quad (26)$$

In (25), the square root function tapers to zero the travelling functions, such reconstructs the appropriate boundary condition. In fact For $l_i > \lambda_{eq}/2$ the tapering occurs with the typical slope of a standing wave. For $l_i \le \lambda_{eq}/2$ the slope is arbitrary but it tends to a linear tapering for very small l_i in terms of the wavelength as a small domain basis function. A nonnegligible advantage of these basis functions is that the Fourier transforms of (22) is in analytical form and can be directly used in a spec-

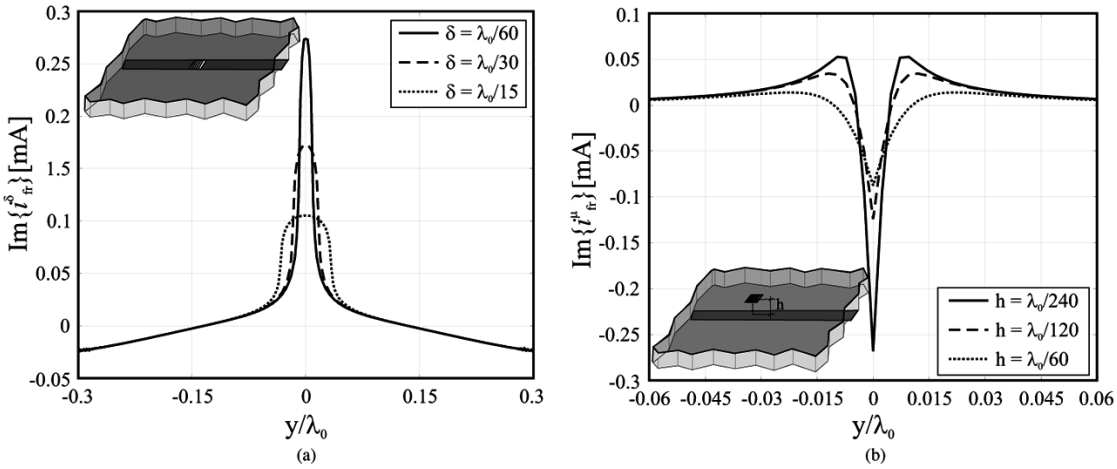

Fig. 4. Imaginary part of the microstrip electric fringe currents ($w_\mu = \lambda_0/60$, $\epsilon_{r1} = 1$, $\epsilon_{r2} = 2.55$). (a) $\mathrm{Im}\left\{i^{\delta}_{fr}\right\}$ (δ-gap feed) for several dimensions of the gap ($h = \lambda_0/120$). (b) $\mathrm{Im}\left\{j^{\mu}_{fr}\right\}$ (Magnetic source feed) for several dielectric thickness.

tral domain mutual couplings. In (22) the rectangular variables (l,t) (which denote *l*onditudinal and *t*ransverse) are (y,x) for the microstrip case and (x,y) for the slot case, respectively. The wave number k_{lpi} is approximated by using in (10) $D \equiv D_\mu$ and $D \equiv D_s$ for the microstrip and the slot, respectively. We denote k_{lpi} as $k_{\mu p}$ and k_{sp} for the two respective cases. For the example under analysis, a total set of ten travelling wave functions have to be included.

B. Fringe Basis Functions

A second type of basis functions is needed to represent the local field behavior around the boundary between uniform regions. These basis functions are shaped as the fringe current defined by applying the regularization process in (12)–(14) to the pertinent canonical problem. The present test case involves four types of fringe basis functions (the real and the imaginary part of the fringe magnetic current on the slot are considered as two different basis functions)

- J_{fr}: it is the fringe electric current on the microstrip for a magnetic source located on the ground plane. Its explicit form is

$$J_{fr}(x,y) = p_t(x,w_\mu) j^{\mu}_{fr}(y) W_{fr}(y) \tag{27}$$

where $W_{fr}(y)$ is a windowing functions which bounds the existence region to the two contiguous uniform regions separated by the discontinuity and introduces in each of the regions a tapering to zero as in (25). In (27)

$$j^{\mu}_{fr} = \frac{1}{2\pi}\int_{-\infty}^{+\infty}\left(\frac{N_\mu(k_y)}{D_\mu(k_y)} - \frac{2k_\mu N_\mu(k_\mu)}{D'_\mu(k_{yp})\left(k_y^2 - k_\mu^2\right)}\right) \times e^{-jk_y(y-y_0)}dk_y \tag{28}$$

where $N_\mu(k_y)$ and $D_\mu(k_y)$ are given in (17) and (18), respectively. No matter what the actual electric field distribution on the slot is, the shape of the electric field impressed on the microstrip will be very similar to the one produced by a unit magnetic dipole placed at the cross over section with length equal to the slot's width. (See inset of Fig. 1). Accordingly, $N_\mu(k_y)$ is modified by multiplying (17) for the spectrum $(P_t(k_y,w_s))$ associated to the above localized source.

- $\widetilde{J}_{fr}$: it is the fringe electric current on the microstrip associated to the δ-gap discontinuity. Its explicit form is

$$\widetilde{J}_{fr}(x,y) = p_t(x,w_\mu) i^{s}_{fr}(y) W(y)$$

where $i^{s}_{fr}(y)$ is formally as in (28) with $D_\mu(k_y)$ as in (18) and

$$N_\mu(k_y) = -\mathrm{sinc}\left(\frac{k_y\delta}{2}\right) P_t(k_y,w_s) e^{jk_y y_0} \tag{29}$$

(this simple form is implied by the fact that the pertinent Green's function becomes a pure exponential term).

The functions j^{μ}_{fr} and i^{s}_{fr} result pure imaginary ($j^{\mu}_{fr} \equiv j\mathrm{Im}\left\{j^{\mu}_{fr}\right\}$, $i^{s}_{fr} \equiv j\mathrm{Im}\left\{i^{s}_{fr}\right\}$) in the example case and they are plotted, with reference to the geometry in Figs. 3 and 4. It is apparent that the fringe currents are always spatially concentrated around the discontinuity, as expected. The reason why these fringe currents are purely imaginary is that the dielectric slab is very thin in terms of the wavelength. If significant radiation would appear this would not be the case. Before proceeding further, we note that the spectrum of the total basis function J_{fr} in (27) is not simply identified through (28), because the truncation function $W(y)$ introduce a spectral convolution by a sinc. For this reason, the spectral domain approach to the MoM reaction integrals is practically not convenient, except for those cases where the the fringe field is completely vanished at the domain truncation.

- M_{fr}: it is the fringe magnetic current on the slot associated to the electric source located at the microstrip level [Fig. 1(b)]. Its explicit form is $m_{fr}(x,y) = p_t(y,w_s) m_{fr}(x) W(x)$ where $W(x)$ is the windowing function as in (27), p_t is defined in (2), and

$$m_{fr}(x) = \frac{1}{2\pi}\int_{-\infty}^{+\infty}\left(\frac{N_s(k_x)}{D_s(k_x)} - \frac{2k_{sp}N_s(k_{sp})}{D'_s(k_{sp})\left(k_x^2 - k_{sp}^2\right)}\right) \times e^{-jk_x(x-x_0)}dk_x \tag{30}$$

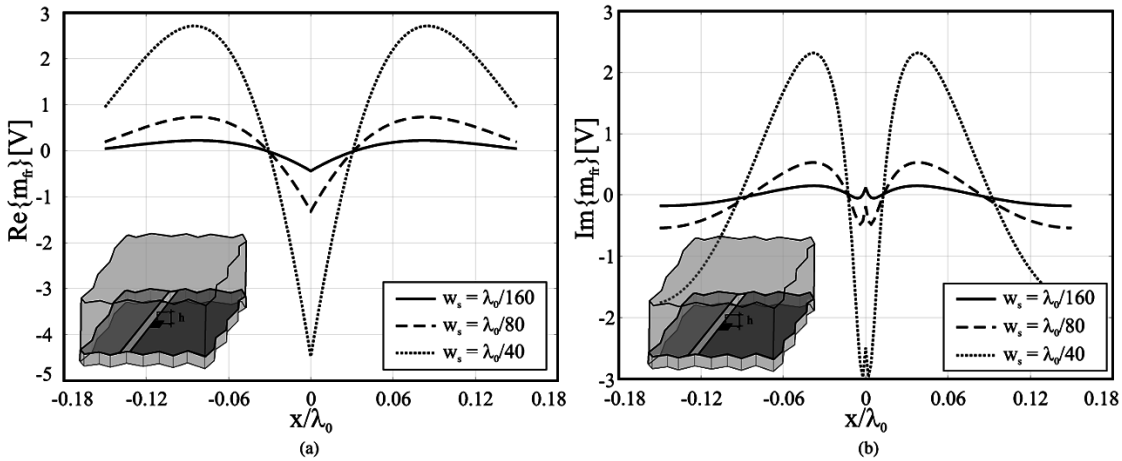

Fig. 5. Slot magnetic fringe currents as a function of the slot width w_s ($w_\mu = \lambda_0/60, h = \lambda_0/120, \epsilon_{r1} = 1, \epsilon_{r2} = 2.55, \epsilon_{r2} = 11.7$). (a) Real part of the slot magnetic fringe current. (b) Imaginary part of the slot magnetic fringe current.

where $N_s(k_x)$ is defined as in (20) except for a multiplication for $P_l(k_x, w_\mu)$.

In this case, two basis functions are defined. One is associated to the real part of the fringe current and one to the imaginary part. The reason why the functions are separate for this case is that the slot radiates. Accordingly, the actual significant contributions are three:

1) leaky waves (described via the travelling waves);
2) space waves (radiated field in the dielectric and in free space);
3) reactive field localized in the surrounding of the source itself.

The fringe functions, being defined as difference between total field and the leaky mode contribution, in this radiating slot case have to account for both the reactive energy (as in the case of the microstrip) and for the space waves. The reactive energy is mostly associated to the imaginary part of the fringe while the space wave is very much associated to the real part of the fringe. This is explained more in detail in a letter [19] authored by two of these same authors. The functions $\mathrm{Re}(m_{fr})$ and $\mathrm{Im}(m_{fr})$ are plotted for the same example in Fig. 5. When the slot's width decreases, $\mathrm{Re}(m_{fr})$ becomes much less significant. It is also worth noting that the fringe contribution associated to the slots do not vanish as rapidly as the one associated to the microstrip; accordingly, its spectrum always require a convolution with a sinc when spectral domain evaluation of the mutual impedances is used.

C. Bend Junctions

Bend junctions deserve special attention. In this work we have used the procedure presented in [14] that includes, directly in the entire domain functions, approximate information on the rapidly varying, vanishing field at the corners. This can be achieved by extending the region in which the basis functions are defined to include the corner regions, and tapering the field with a linear profile to zero [14, Fig. 6]. Despite the reasonable flexibility not all common dipole or slot based structures can be studied using this methodology at the present time. In particular structures with rapidly and continuously varying cross sections such as bow tie dipoles or slots or gradual matching networks, would render the separability of the variables in the current distribution discussible.

IV. MoM Analysis

Once the basis functions to represent the problem are introduced, the reaction integrals are evaluated as in any conventional MoM procedure. The reaction integrals can be conveniently evaluated in the space domain for terms involving fringe functions since these latter have a broad spectrum. The spectral domain is more convenient when calculating the coupling between travelling waves, which possess a concentrated spectrum. The results presented next are obtained by a spatial domain approach for the mutual impedance calculation. The results are compared with those obtained by a conventional subdomain full-wave code developed in house and by Ansoft Designer.

Since the informations on the reactive energy (rapid field variations) associated to feeds and discontinuities are directly incorporated in the fringe basis functions, the number of basis functions needed is drastically reduced, with evident advantage of both computing time and memory needed especially for large arrays.

A. Resonant Microstrip-Coupled Slot

The solution for the test case of Fig. 3 is presented in Fig. 6(a) and (b), relevant to the electric currents on the microstrip and the magnetic currents on the slot, respectively. The different blocks in which the structure is partitioned are indicated below the horizontal scale. The results from our method are successfully compared with those from a conventional subdomain method which make use of piece wise linear subdomain basis functions.

Fig. 7 presents the total magnetic current (continuous line) on the resonant slot, together with the individual contributions from each of the basis functions. For the slot it is apparent that the two travelling waves alone, cannot adequately reconstruct the total current. In particular, at the cross section with the microstrip,

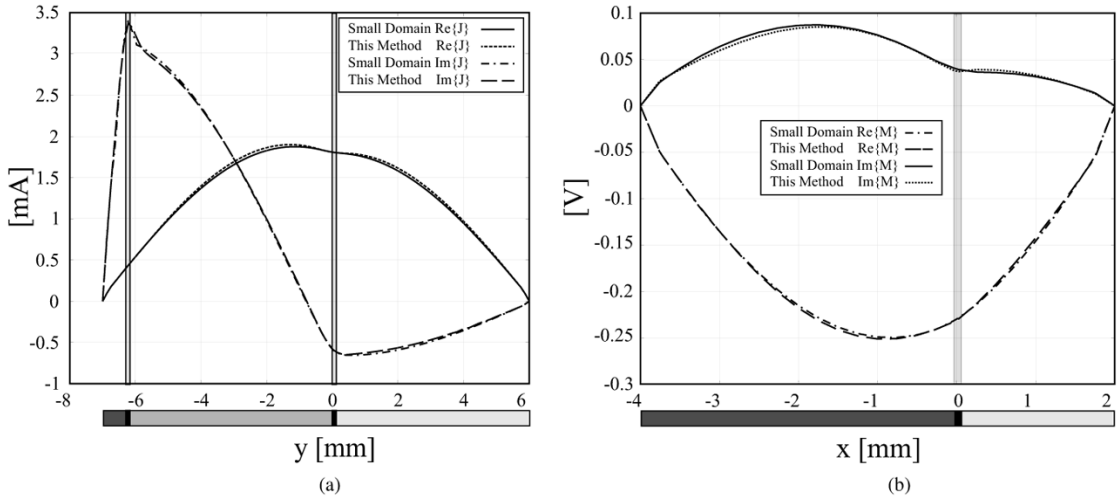

Fig. 6. Electric and magnetic currents for the geometry shown in Fig. 3 ($f = 9\,\mathrm{Ghz}$, $w_\mu = 0.5\,\mathrm{mm}$, $l_\mu = 6\,\mathrm{mm}$, $w_s = 0.4\,\mathrm{mm}$, $l_s = 2\,\mathrm{mm}$, $h = 0.275\,\mathrm{mm}$, $\epsilon_{r1} = 1$, $\epsilon_{r2} = 2.55$, $\epsilon_{r3} = 11.7$).(a) Real and imaginary part of the microstrip electric current. (b) Real and imaginary part of the slot magnetic current.

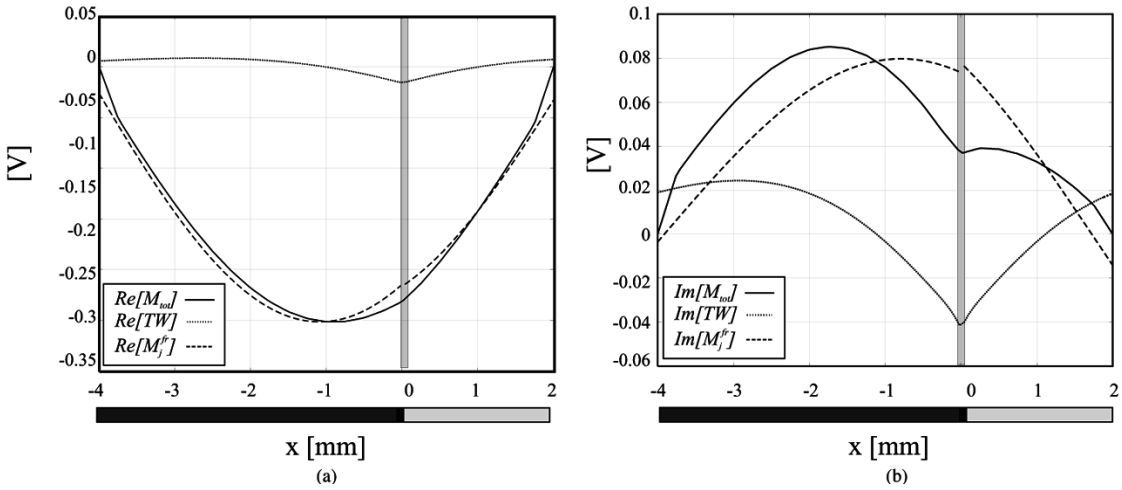

Fig. 7. (a) Real part and (b) imaginary part of the total slot current (continuous line), of the travelling waves (dashed line) and of the fringe currents (dotted line) ($f = 9$ Ghz, $w_\mu = 0.5\,\mathrm{mm}$, $l_\mu = 6\,\mathrm{mm}$, $w_s = 0.4\,\mathrm{mm}$, $l_s = 2\,\mathrm{mm}$, $h = 0.275\,\mathrm{mm}$, $\epsilon_{r1} = 1$, $\epsilon_{r2} = 2.55$, $\epsilon_{r3} = 11.7$).

the fringe functions m_{fr} neatly reconstructs the locally reactive shape of the magnetic current. Note that the fringe current may not be an accurate approximation for the continuous-spectrum current on a piece of strip conductor when the strip extends beyond the slot discontinuity only a small amount. This is because reflections of the continuous-spectrum current at the ends of the strip are ignored—the fringe current is simply a truncated version of the continuous spectrum current on an infinite strip. However, in all examples treated such a problem was never found to impact significantly in the results.

It is clear that the advantage in terms of calculation time and memory allocation in this case of a single resonant element is not particularly important, nevertheless the advantages in nonresonant geometries Section IV-B and array configurations Section IV-C will be more evident.

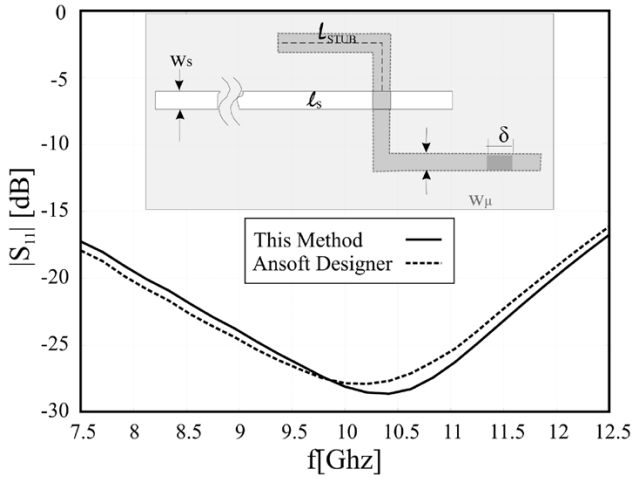

Fig. 8. S parameter for microstrip fed slot ($l_s = 90\,\mathrm{mm}$, $w_s = 0.4\,\mathrm{mm}$, $l_{\mathrm{stub}} = 5.6\,\mathrm{mm}$, $w_\mu = 0.7\,\mathrm{mm}$, $\delta = 2.1\,\mathrm{mm}$, $h = 0.275\,\mathrm{mm}$, $\epsilon_{r1} = 1$, $\epsilon_{r2} = 2.55$, $\epsilon_{r3} = 11.7$).

B. Nonresonant Microstrip-Coupled Leaky-Wave Slot

In this section we investigate a long slot coupled to a bent microstrip, this latter fed by a δ-gap (see Fig. 8). The structure realizes a leaky-wave slot antenna, whose basic physical properties have been investigated in [16]. The slot is printed between a homogeneous half-space of relative permittivity 11.7, and a dielectric slab of relative permittivity 2.55 and thickness

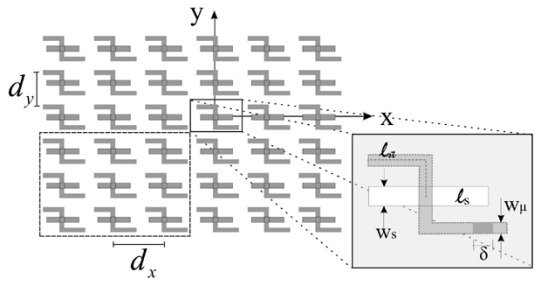

Fig. 9. 6×6 array of microstrip fed slots ($l_s = 6.6$ mm, $w_s = 0.3$ mm, $l_\mu = 7.25$ mm, $w_\mu = 0.5$ mm, $\delta = 1.5$ mm, $d_x = 9$ mm, $d_y = 6$ mm, $h = 0.275$ mm, $\epsilon_{r1} = 1, \epsilon_{r2} = 2.55, \epsilon_{r3} = 11.7$).

0.275 mm. The amplitude of the reflection coefficient S_{11} at the input port obtained by our method is compared with that obtained by Ansoft Designer. (Note that the use of the travelling basis functions allows for a natural definition of the reflection coefficient).

In the example of Fig. 8, the microstrip line present two bends, as well as all the elements of the array in Fig. 9. In this case the selection of the fringe basis functions is still as the one described in Section III. Thus the fringe functions are associated only to the δ-gap excitation and to the cross over between the slot and the microstrip. However a couple of entire domain basis functions is defined in each of the discontinuity free pieces of microstrip regions (in total 8 travelling wave functions).

It should be noted that for long antennas (as this one) the gain in terms of reduction of unknown number is really significant. Only 6 entire domain basis functions are included in the slot against 150 subdomain functions of the conventional approach. The actual dimensions of the case reported in Fig. 8 were taken just as an example. It is worth noting that if the width of the exciting microstrip w_μ was 0.07 mm rather than 0.7 mm the number of entire domain basis functions would have remained 6 while the number of subdomain functions would have been 1500. This independence from the dimensions of the small details is the most significant advantage of the proposed method.

C. Slot Arrays

The use of travelling wave and fringe wave basis functions is particulary beneficial in array problems. The simultaneous presence of subwavelength details implies for conventional analysis, a subwavelength meshing which should be maintained on the overall large dimension of the array. The consequent high number of unknowns often render the problem intractable.

In the present approach, the subwavelength details are incorporated in the fringe currents basis functions, which therefore dominate the short-range interaction. This allows to establish a robust criterion to drop off the mutual impedance associated to the fringe contributions for large distance. On the other hand, the travelling wave basis functions contributions dominate the large distance interaction. Eventually, the dramatic saving of computation time is not only due to reduction of the linear system inversion time reduction but also to the reduction of filling time.

Consider the array shown in Fig. 9, composed by microstrip-fed slots printed on a ground plane that separates a

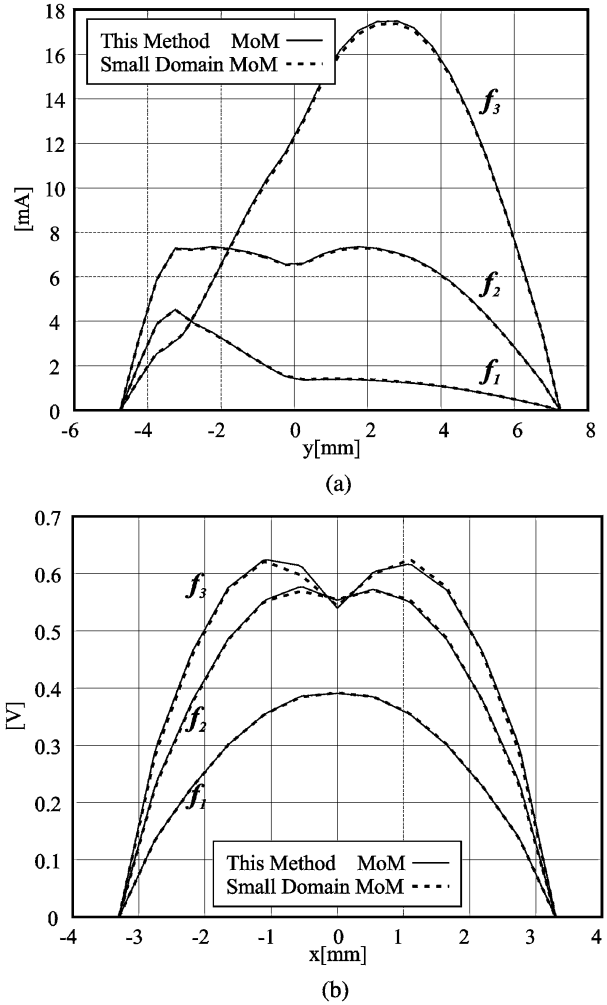

Fig. 10. Amplitude of the currents for the center element of the 3×3 array. (a) Electric current on the microstrip. (b) Magnetic currents on the slot.

homogeneous silicon half space ($\epsilon_r = 11.9$) from a dielectric slab ($\epsilon_r = 2.55$, $h = 0.275$ mm) where the microstrips are printed. The slot's length and width are 6.6 and 0.3 mm, respectively. The microstrip is bent for reason of reduced space, since the periodicity of the array in the E-plane, designed for imaging applications, should be small. The periodicities are 9 mm in the x-direction and 6 mm in the y-direction. The microstrip's stub which excitates the slot is of length 7.25 mm and the microstrip's width is 0.5 mm. Let uss first consider a subarray of 3×3 elements framed by dashed line in Fig. 9. Entire domain MoM results and conventional subdomain MoM results are compared for the central element in Fig. 10 and for the upper right element in Fig. 11. The amplitude of the currents on slots and microstrips are shown for three different frequencies ($f_1 = 8.8$ GHz, $f_2 = 9.86$ GHz, $f_3 = 11.2$ GHz). Fig. 12 shows the active reflection coefficients on different elements of the 3×3 array. The elements of the upper and lower rows have almost the same reflection coefficient, which is around -12 dB. In the central row, where the coupling in the y-direction is stronger, the minimum increases to -8 dB. The conventional MoM results presented in Figs. 10 and 11 are obtained by our in-house developed code based on subdomain basis functions, which does not allow by to treat the total 6×6

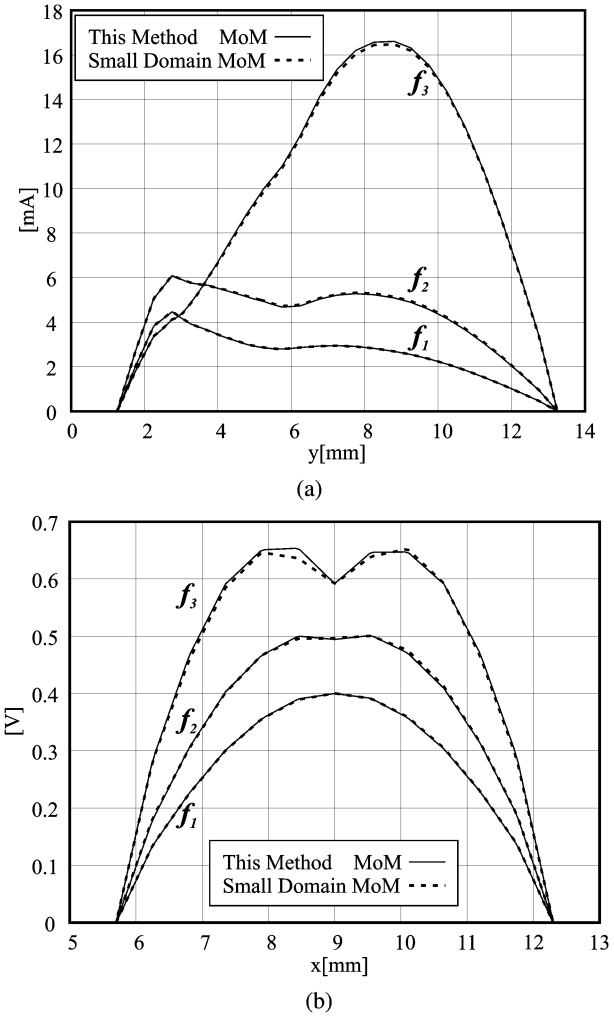

Fig. 11. Amplitude of currents for the upper right element of the 3×3 array. (a) Electric current on the microstrip. (b) Magnetic currents on the slot.

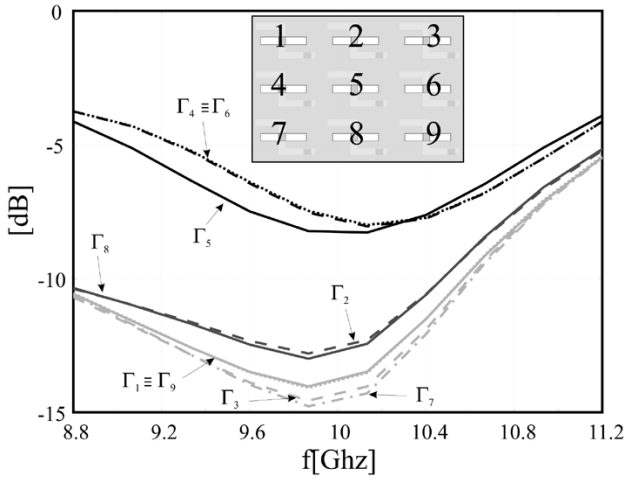

Fig. 12. Active reflection coefficients on the array elements.

array shown in Fig. 9 with significant accuracy. To provide reference results for the 6×6 array we have used Ansoft Designer. The amplitude of the active reflection coefficient for the corner

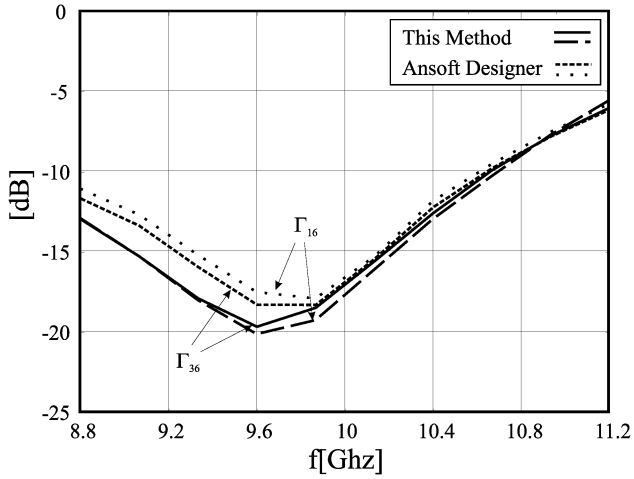

Fig. 13. Reflection coefficient of the 6×6 array (indicated in Fig. 10) on the central element and on the down right corner element.

slot (Γ_{36}) and for the central slot (Γ_{16}) (which is that with the zoom in Fig. 9) is presented in Fig. 13. The discrepancy (that appears only at lower frequencies) could be attributed to a ill conditioning of the subdomain based MoM matrix calculated by the commercial code. It could appear a contradiction that the condition of the matrix is worse at lower frequencies since the object is smaller in terms of the wavelength. However if one uses a uniform mesh the number of unknowns is only dictated by the smallest dimension involved and not by the frequency. Thus, even if the number of functions remains the same the accuracy and the conditioning of the matrix become worse due to the fact that the couplings at low frequencies involve larger reactive energy.

V. Conclusion

A method has been presents for the analysis of arrays whose BFN and radiating elements are composed of pieces of planar and uniform transmission lines. The main advantageous feature of the basis functions used is their splitting into fringe wave and travelling wave components, which are associated to different properties of the coupling phenomena. Differently with respect to many other MoM techniques, the entire domain basis functions have to be generated numerically. The solution to a different set of canonical problems for each structure to be investigated is required. Nevertheless the methodology is fairly automatic. The key aspect is that one is required to generate a database of software functions that solve a number of canonical problems defined by some key parameters. Once the data base is available the technique is straight forward. A specific example structure composed of slot elements fed by microstrips has been investigated in detail. For this case, the method has been validated against element by element codes showing excellent accuracies and significant improvements for both calculation times and memory occupations requirements. The method is indeed particularly well suited for analyzing integrated antennas in which the BFN cannot naturally be separated from the radiating elements. The applications in which this happens more often are in integrated receivers at millimeter and submillimeter

wave frequencies where small dimension of δ-gap well represent realistic devices (mixer or direct detector).

The method is also particularly useful for the analysis of printed slot reflect-arrays, where each element is loaded by a microstrip.

ACKNOWLEDGMENT

Gratitude is expressed to an anonymous reviewer for accurate and useful suggestions.

REFERENCES

[1] N. Engheta, W. D. Murphy, V. Rokhlin, and M. S. Vassiliou, "The fast multipole method (FMM) for electromagnetic scattering problems," *IEEE Trans. Antennas Propag.*, vol. 40, no. 6, pp. 634–641, Jun. 1992.

[2] E. Michielsenn and A. Boag, "A multilevel matrix decomposition algorithm for analyzing scattering from large structures," *IEEE Trans. Antennas Propag.*, vol. 44, no. 8, pp. 1086–1093, Aug. 1996.

[3] P. Pirinoli, G. Vecchi, and L. Matekovits, "Multiresolution analysis of printed antennas and circuits: A dual-isoscalar approach," *IEEE Trans. Antennas Propag.*, vol. 49, no. 6, pp. 858–874, Jun. 2001.

[4] A. Neto, S. Maci, G. Vecchi, and M. Sabbadini, "A truncated floquet wave diffraction method for the full-wave analysis of large phased arrays—Part I: Basic principle and 2-D case," *IEEE Trans. Antennas Propag.*, vol. 48, no. 4, pp. 594–600, Apr. 2000.

[5] ——, "A truncated floquet wave diffraction method for the full-wave analysis of large phased arrays. Part II: Generalization to 3-D cases," *IEEE Trans. Antennas Propag.*, vol. 48, no. 4, pp. 601–611, Apr. 2000.

[6] A. Cucini, M. Albani, and S. Maci, "Truncated floquet wave full-wave $(\mathrm{T(FW)^2})$ analysis of large periodic arrays of rectangular waveguides," *IEEE Trans. Antennas Propag.*, vol. 51, no. 6, pp. 1373–385, Jun. 2003.

[7] ——, "Truncated floquet wave full-wave analysis of large phased arrays of open-ended waveguides with a nonuniform amplitude excitation," *IEEE Trans. Antennas Propag.*, vol. 51, no. 6, pp. 1386–1394, Jun. 2003.

[8] L. Matekovits, G. Vecchi, G. Dassano, and M. Orefice, "Synthetic function analysis of large printed structures: The solution space sampling approach," in *Dig. IEEE Antennas and Propagation Soc. Int. Symp.*, Boston, MA, Jul. 8–13, 2001, pp. 568–571.

[9] P. Focardi, A. Freni, S. Maci, and G. Vecchi, "Efficient analysis of arrays of rectangular corrugates horns: The synthetic aperture function approach," *IEEE Trans. Antennas Propag.*, vol. 53, no. 2, pp. 601–607, Feb. 2005.

[10] S. Maci, G. Vecchi, and A. Freni, "Matrix compression and supercompression techniques for large arrays," in *Proc. IEEE Antennas and Propagation Soc. Int. Symp.*, vol. 2, Jun. 22–27, 2003, pp. 1064–1067.

[11] P. Pirinoli, L. Matekovits, G. Vecchi, F. Vipiana, and M. Orefice, "Synthetic functions, multiscale MoM analysis of arrays," in *IEEE Antennas and Propagation Soc. Int. Symp.*, vol. 4, Jun. 22–27, 2003, pp. 799–802.

[12] V. V. S. Prakash and R. Mittra, "Characteristic basis function method: A new technique for fast solution of integral equations," *Microw. Opti. Technol. Lett.*, pp. 95–100, Jan. 2003.

[13] R. Mittra, "A proposed new paradigm for solving scattering problems involving electrically large objects using the characteristic basis functions method (CBF)," in *Proc. Int. Conf. Electromagnetics in Advanced Applications (ICEAA'03)*, Turin, Italy, Sep. 8–12, 2003, pp. 621–623.

[14] A. Neto, P. J. De Maagt, and S. Maci, "Optimized basis functions for slot antennas excited by coplanar waveguides," *IEEE Trans. Antennas Propag.*, vol. 51, no. 7, pp. 1638–1646, Jul. 2003.

[15] A. Neto and S. Maci, "Green's function of an infinite slot printed between two homogeneous dielectrics—Part I: Magnetic currents," *IEEE Trans. Antennas Propag.*, vol. 51, no. 7, pp. 1572–1581, Jul. 2003.

[16] ——, "Green's function of an infinite slot line printed between two homogeneous dielectrics—Part II: Uniform asymptotic fields," *IEEE Trans. Antennas Propag.*, vol. 52, no. 3, pp. 666–676, Mar. 2004.

[17] D. R. Jackson, F. Mesa, C. Di Nallo, and D. P. Nyquist, "The theory of surface-wave and space-wave leaky-mode excitation on microstrip lines," *Radio Sci.*, vol. 35, pp. 495–510, Mar.-Apr. 2000.

[18] P. C. Clemmow, *The Plane Wave Spectrum Representation of Electromagnetic Fields*, 2nd ed. Piscataway, NJ: IEEE Press, 1996, ch. 4.

[19] A. Neto and S. Maci, "Input impedance of slots printed between two dielectric media and fed by a small δ-gap," *IEEE Antennas Wireless Propag. Lett.*, vol. 3, pp. 113–116, 2004.

Simona Bruni received the Laurea degree in telecommunications engineering from the University of Siena, Siena, Italy, in 2002.

Since 2002, she has been working toward the Ph.D. degree in electromagnetic engineering with the Department of Information Engineering, University of Siena. Her Ph.D. degree work is financed and hosted by the Defence, Security and Safety Institute of the Netherlands Organization for Applied Scientific Research (TNO), The Hague. Her research interests are in the area of applied electromagnetics, focused on numerical and asymptotic methods, and design of broad-band directive antennas.

Ms. Bruni's doctoral Ph.D. studies are financed and hosted by the Defence, Security and Safety Institute of the Netherlands Organization for Applied Scientific Research (TNO), The Hague.

Nuria Llombart received the Ingeniero de Telecomunicación degree from the Universidad Politécnica de Valencia, Spain, in 2002. She is working toward the Ph.D. degree at the same university.

She spent one year, 2000 to 2001, at the Friedrich-Alexander University of Erlangen-Nuremberg, Germany, and worked at Fraunhofer Institute for Integrated Circuits in Erlangen, Germany, from 2000 until 2002. Her current research interests include numerical and analytical methods for the analysis and design of printed antennas and EBG structures.

Ms. Llombard's Ph.D. studies are financed and hosted by the Defence, Security and Safety Institute of the Netherlands Organization for Applied Scientific Research (TNO) in The Hague, The Netherlands.

Andrea Neto (M'00) received the Laurea degree (*summa cum laude*) in electronic engineering from the University of Florence, Florence, Italy, in 1994 and the Ph.D. degree in electromagnetics from the University of Siena, Siena, Italy, in 2000. Part of his Ph.D. degree dissertation was developed at the European Space Agency Research and Technology Center (ESTEC), Noordwijk, The Netherlands.

For two years, he worked in the Antenna Section at the European Space Agency Research and Technology Center (ESA-ESTEC), Noordwijk, The Netherlands. From 2000 to 2001, he was a Postdoctoral Researcher with the S.W.A.T. Group of the Jet Propulsion Laboratory, California Institute of Technology, Pasadena. Since 2002, he has been a Senior Antenna Scientist with the Netherlands Organization for Applied Scientific Research (TNO) Defence, Security and Safety, The Hague, The Netherlands. His research interest is concerned with analytical and numerical methods applied to antennas and microwave circuits, with emphasis on large printed arrays and dielectric lens antennas.

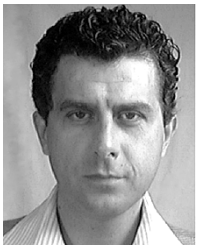

Giampiero Gerini (M'92) received the M.S. degree (*summa cum laude*) and the Ph.D. degree in electronic engineering from the University of Ancona, Ancona, Italy, in 1988 and 1992, respectively.

From 1994 to 1997, he was Research Fellow at the European Space Research and Technology Centre (ESA-ESTEC), Noordwijk, The Netherlands, where he joined the Radio Frequency System Division. Since 1997, he has been with the Netherlands Organization for Applied Scientific Research (TNO), The Hague, The Netherlands. At TNO Defence, Security and Safety, he is currently Chief Senior Scientist of the Antenna Unit in the Transceivers and Real-time Signal Processing Department. His main research interests are phased array antennas, frequency selective surfaces, and integrated front-ends.

Stefano Maci (M'92–SM'99–F'04) was born in Rome, Italy. He received the Laurea degree *(cum laude)* in electronic engineering from the University of Florence, Italy, in 1987.

From 1990 to 1998, he was with the Department of Electronic Engineering, University of Florence, as an Assistant Professor. Since 1996, he has been responsible for the University of Siena, Siena, Italy, projects supported by the European Community and the European Space Agency. In 1997, he was an Invited Professor at the Technical University of Denmark, Copenhagen. In 1998, he joined the Department of Information Engineering, University of Siena, as an Associate Professor. He is currently responsible for several research contracts and projects supported by national and international institutions. In the sixth EU framework program he is responsible of the European School of Antennas of the Antenna Center of Excellence. He is the principal author or coauthor of about 40 papers in IEEE TRANSACTIONS, 40 papers in other international journals, and more than 200 papers in proceedings of international conferences. He was coauthor of an incremental theory of diffraction, which describes a wide class of electromagnetic scattering phenomena at high frequency, and of a diffraction theory for the high-frequency analysis of large truncated periodic structures. His research interests are focused on electromagnetic engineering, mainly concerned with high-frequency ad numerical methods for antennas and scattering problems.

Prof. Maci is a Member of the Technical Advisory Board of the International Scientific Radio Union (URSI) Commission B, and the Advisory Board of the Italian Ph.D. School of Electromagnetism. He received the "Barzilai" prize for the best paper at the Italian National Electromagnetic Conference (XI RiNEm) in 1996. He was Associate Editor of the URSI disk of reference from 1996 to 1999, Associate Editor of IEEE TRANSACTIONS ON ELECTROMAGNETIC COMPATIBILITY from 1999 to 2001, and Convenor at the URSI General Assembly in 2002. He was Chairman and Organizer of several special sessions at international conferences and has been Chairman of two international workshops. He was a Guest Editor of the IEEE TRANSACTIONS ON ANTENNAS AND PROPAGATION *Special Issue on Artificial Magnetic Conductors, Soft Hard Surfaces, and Other Complex Surfaces*.